Received: 18 January 2024 | Revised: 1 May 2024 | Accepted: 4 May 2024

DOI: 10.1002/est2.637

RESEARCH ARTICLE

ENERGY STORAGE WILEY

Exploring the influence of Ni doping thin films for supercapacitor application

V. B. Ranmale[1] | L. D. Kadam[2] | T. J. Shinde[3]

[1]Department of Physics, Swami Ramanand Vidyalaya and Junior College Ramanandnagar (Burli), Sangli, India

[2]Department of Physics, Rajarshi Chh. Shahu College, Kolhapur, India

[3]Department of Physics, Smt. KRP Kanya Mahavidyalaya, Islampur, India

Correspondence
V. B. Ranmale, Department of Physics, Swami Ramanand Vidyalaya and Junior College Ramanandnagar (Burli), Sangli 416308, India.
Email: vb_ranmale@yahoo.co.in

Abstract

This study explores the impact of nickel (Ni) doping bismuth ferrite ($BiFeO_3$) thin film synthesis by spray pyrolysis method. The structural and morphological study shows that the thin films are slightly amorphous with granular morphology. Investigated the supercapacitive behavior of synthesized material by using cyclic voltammetry, galvanostatic charge-discharge, and electrochemical impedance spectroscopy. The thin films synthesized are capable of storing a 253.31 F/g capacitance at a 10 mV/s scan rate and by introducing nickel into the synthesis process, we obtained 312.12 F/g capacitance at a 10 mV/s scan rate. The material shows good cyclic stability after 91000 cycles. It is also observed that no structural and morphological changes were made by doping Ni into $BiFeO_3$ thin films. The significant improvement in capacitance was displayed by Ni doping into $BiFeO_3$ obtained via spray pyrolysis methods indicating its potential for use in supercapacitor applications.

KEYWORDS

bismuth ferrite; Ni doping, spray pyrolysis; supercapacitor

1 | INTRODUCTION

The increasing worldwide need for energy has directed research efforts toward the development of improved energy storage systems capable of achieving rising power demands while also addressing environmental issues.[1,2] In comparison to conventional energy storage options, supercapacitors have emerged as promising devices with high-power density, quick charge-discharge cycles, and long-term operating lifetimes.[3,4] Their ability to bridge the gap between short-term high-power demands and long-term energy storage has led to increased research and development in electrochemical energy storage.

Among the several materials under consideration for supercapacitor applications, $BiFeO_3$ has received significant attention because of its multifunctional features, which include strong ferroelectricity, multiferroicity, and great chemical stability.[5,6] These properties make $BiFeO_3$ a fascinating option for energy storage applications, notably supercapacitors, where high energy densities and outstanding charge storage capacities are essential.

Synthesizing thin films of $BiFeO_3$ gives a possible path for improving its efficacy in supercapacitor technology.[7,8] The spray pyrolysis process is one significant technology gaining interest in the synthesis of $BiFeO_3$ thin films.[9,10] This technology is known for its simplicity of use, scalability, low cost, and ability to synthesize thin films with controlled thickness and composition. Unlike other processes, spray pyrolysis allows for straightforward doping, making it possible to use dopants such as Ni to modify the electrical properties of $BiFeO_3$ thin films for improved supercapacitor performance.[11,12]

Theoretical specific capacitance values for bismuth ferrites vary between approximately 925 and 1233 F g^{-1}, which correspond to either three or four electron transfer reactions.[13] However, despite these encouraging numbers, spinel ferrites demonstrate not enough electrical conductivity and slow ion diffusion.[14] In order to

overcome this limitation, our study aims to fill a substantial gap in the current knowledge. Our research focuses on studying the synthesis, characterization, and electrochemical behavior of spray synthesized thin films doped with Ni in $BiFeO_3$. Our research focuses on improving the performance of supercapacitors by conducting a detailed analysis of the impact of Ni doping using the spray pyrolysis technique. Through our work, we aim to push forward the progress of energy storage systems that are both efficient and sustainable.

1.1 | Experimental details

Nickel-doped bismuth ferrite thin film ($BiFeO_3$) was synthesized by spray pyrolysis technique. The bismuth nitrate, iron nitrate, and nickel nitrate with stoichiometric proportion, were dissolved in double distilled water at room temperature using a magnetic stirrer, in a 1:1 ratio. The solution was sprayed onto FTO (FTO with approx. 2 Ω /cm^2 sheet resistance) heated substrate, which was maintained at a temperature of 310°C. The spraying nozzle was positioned 10 cm away from the top of the substrate, and the solution was sprayed in a cone-shaped pattern. The films were deposited using a solution flow rate of 1 mL/min and a carrier gas pressure of 2 kg/cm^2. Subsequently, these films were subjected to post-annealing at 310°C for 1 h.

The synthesized films are characterized by X-ray diffraction (XRD) using an advanced Bruker D8 diffractometer with CuKα radiation. The crystalline size of the BFO films has been calculated by using the Debey Scherrer Formula:

$$D = \frac{K\lambda}{\beta \cos\theta}, \quad (1)$$

where D is the crystalline size, K is the constant (0.9), λ is the x-ray wavelength, β is the fill length half maximum intensity, and θ is the Bragg angle. The morphological analysis was carried out on a JEOL (JSM-IT200) microscope with EDAX. An Autolab electrochemical workstation equipped with a three-electrode setup was used to perform electrochemical properties. A synthesized thin film was used as the working electrode in this arrangement, while an Ag/AgCl electrode was used as the reference electrode and a platinum wire as the counter electrode.

2 | RESULT AND DISCUSSION

Through the XRD analyses performed on the Ni-doped $BiFeO_3$ nanocomposite, as shown in Figure 1, valuable information regarding its structural properties, crystallinity, and purity was obtained. The XRD patterns showed

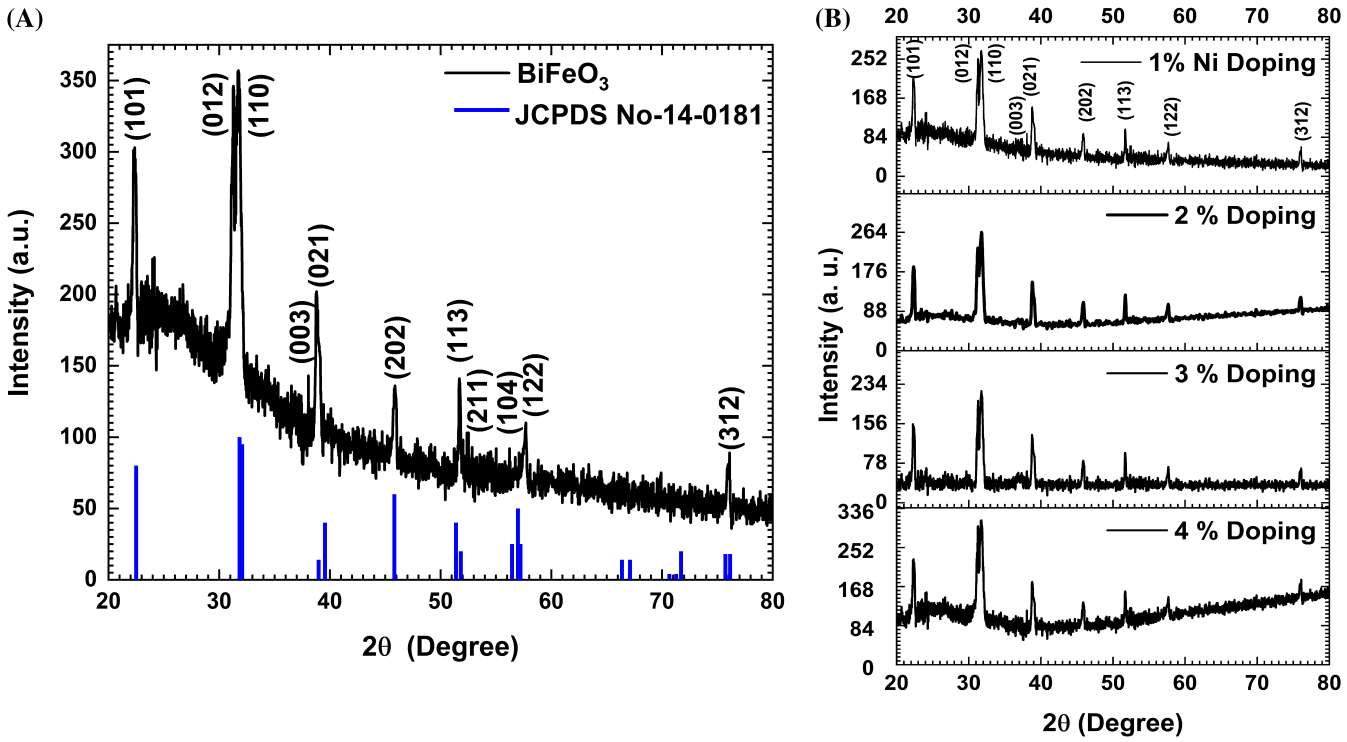

FIGURE 1 XRD pattern of (A) pure $BiFeO_3$ and (B) Ni doped $BiFeO_3$ thin films powder obtained from film. XRD, X-ray diffraction

clear peaks at different 2θ values, including 22.31°, 31.28°, 31.78°, 38.15°, 38.94°, 45.88°, 51.61°, and 57.68°, which corresponded to specific Miller planes such as (101), (012), (110), (003), (021), (202), (113), and (122). These peaks confirm the presence of the rhombohedral perovskite phase (R3c) characteristic of $BiFeO_3$, in accordance with the JCPDS no. 14-0181.[15,16] It is intriguing how the addition of Nickel (Ni) ions into the $BiFeO_3$ lattice caused slight changes in its crystal structure.[17-19] This phenomenon is likely due to the partial transformation of the Bi-O bond into the Ni-O bond, which is made possible by the partial substitution of Bi^{3+} ions with Ni^{2+} ions.[20] As a result, the crystal lattice experienced a decrease in the number of oxygen vacancies, resulting in an improvement in the material's electrical conductivity. In addition, the XRD analysis showed a slight change in diffraction angle towards higher values (~32°) after the introduction of Ni^{2+} ions, suggesting a possible modification in the crystal phase structure.[21] This observation emphasizes the complex relationship between dopant ions and the host lattice, showcasing the ability to customize the structural and electrical properties of $BiFeO_3$-based materials through precise doping techniques. Insights obtained from XRD analyses play a crucial role in enhancing our comprehension of the fundamental processes that dictate the structural changes and functional characteristics of intricate oxide nanocomposites.

The microphotograph of Ni-doped $BiFeO_3$ thin film is displayed in Figure 2A-D. The scanning electron microscopy (SEM) examination showed that the aggregated nanoparticles varied in size from 50 to 70 nm, which closely matched with results obtained from the XRD results. In addition, by utilizing the SEM-energy-dispersive X-ray spectroscopy technique, the Bi/Fe ratio was determined. The obtained graph shown in Figure 3 values were found to be within an acceptable range considering the precision of the technique and were consistent with previous studies. This suggests potential advantages for improved performance in energy storage devices such as supercapacitors.[22] Even with the addition of different amounts of Ni as a dopant, the $BiFeO_3$ thin layers maintained their original structure, highlighting the preservation of beneficial voids. The remarkable morphology and enhanced conductivity achieved through Ni doping highlight the promising potential of Ni-doped $BiFeO_3$ for advanced energy storage applications.

Using transmission electron microscopy (TEM), valuable information was obtained about the microstructure of nickel-doped bismuth ferrite ($BiFeO_3$), revealing intricate details about its crystallographic features. TEM analysis, shown in Figure 2E-H, unveiled the spacing of neighboring lattice fringes in the original nickel-doped $BiFeO_3$, measuring about 0.284 nm, which aligns with the (101) and (012) planes of pure $BiFeO_3$.[23] This observation emphasizes the strong structural integrity of the doped material, indicating that the crystalline lattice remains largely undisturbed with the addition of nickel. Examining the crystal structure, Figure 2E-H presents high-resolution TEM images captured along the (101) zone axis. These images offer additional confirmation of the crystal structure and reveal subtle changes caused by nickel doping.[24] Through careful examination of the images, subtle changes in the atomic arrangement were observed, confirming the existence of nickel ions within the $BiFeO_3$ lattice and their influence on the crystallographic configuration.[25] Understanding the atomic-scale modifications highlights how TEM analysis can detect even the most subtle structural changes caused by incorporating dopants. The presence of rhombohedral phases in the nickel-ion-doped $BiFeO_3$ samples was revealed through Fourier transform (FT) analysis, as shown in Figure 6. This discovery aligns with the expected results from XRD analysis, confirming the high quality of the $BiFeO_3$ phase produced using the spray pyrolysis technique. The correlation between TEM and XRD findings highlights the trustworthiness of TEM in determining the crystalline phases and purity of the synthesized material. Through TEM analysis, a thorough examination of the microstructural properties of nickel-doped $BiFeO_3$ was conducted, revealing important details about its crystallography and phase composition. These findings improve our understanding of the structural properties of doped $BiFeO_3$ and highlight the effectiveness of TEM as a powerful tool for nanoscale characterization in materials science research.

Through the use of X-ray photoelectron spectroscopy (XPS) analysis, as shown in Figure 4, the complex composition and structural features of nickel-doped bismuth ferrite ($BiFeO_3$) thin films were revealed. These films were synthesized with the aim of exploring their potential applications in electrochemical energy storage. Through careful curve fitting of the XPS spectra, the valence states of metal ions and oxygen vacancies within the material were determined. The peaks of Bi 4f, Fe 2p, Ni 2p, and O 1s were analyzed in detail. There were subcomponents observed in the Bi 4f peaks at binding energies of 161.66 and 167.27 eV, which corresponded to Bi 4f 5/2 and Bi 4f 7/2, respectively.[26] This suggests the presence of Bi^{3+} ions. We observed that the Fe 2p peaks showed characteristics associated with Fe^{2+} and Fe^{3+} species. These were further supported by the presence of satellite peaks at different binding energies. Confirming successful nickel incorporation into the $BiFeO_3$ lattice, the Ni 2p peaks were assigned to Ni^{3+} ions at a binding energy of 854.77 and 872.59 eV are Ni 2p 3/2 and Ni 2p

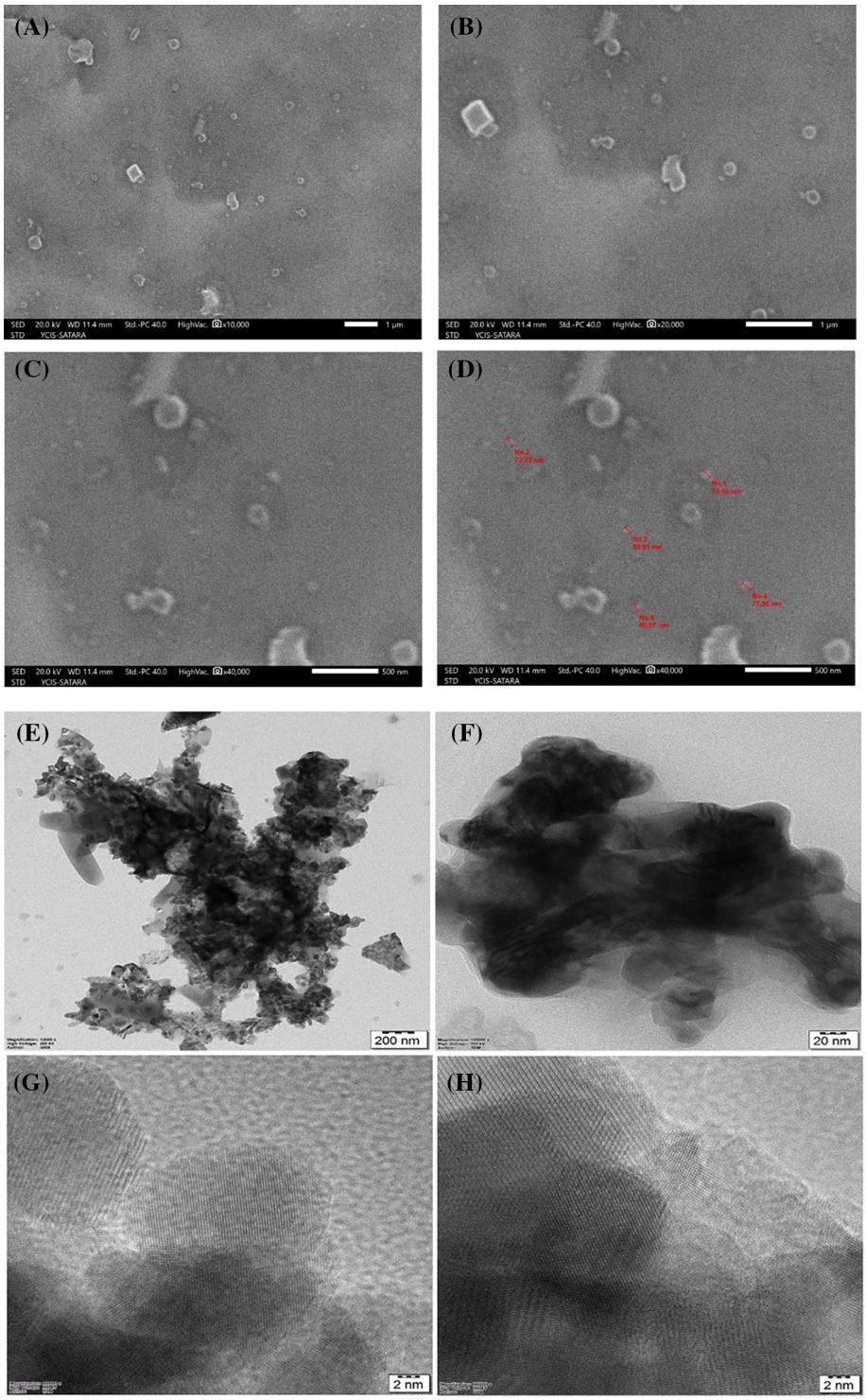

FIGURE 2 (A-D) SEM images and (E-H) TEM images of as synthesized thin film of $BiFeO_3$ with different magnifications. SEM, scanning electron microscopy; TEM, transmission electron microscopy

1/2, respectively. Upon analyzing the O 1 s spectra, it was observed that there were peaks indicating the presence of lattice oxygen (O L), oxygen vacancies (O V), and surface oxygen (OH). The surface oxygen was attributed to hydroxide groups resulting from Lewis acidity at oxygen vacancy sites.[27] Interestingly, the Ni-doped $BiFeO_3$ samples showed higher levels of lattice oxygen, suggesting improved crystallinity, as supported by XRD findings. The compact atomic structure and increased oxygen content play a crucial role in enhancing the electrical conductivity and rate capability of metal oxide electrodes used in electrochemical energy storage applications. With careful XPS analysis, the composition and structural details of the synthesized thin films were clearly determined, enhancing their potential use in advanced supercapacitor technologies. These findings confirm the

successful integration of nickel into the $BiFeO_3$ lattice and offer valuable insights into the charge compensation mechanism and oxygen vacancy dynamics within the material. Thorough characterization is crucial in customizing the properties of electrode materials to meet the rigorous demands of high-performance energy storage devices. XPS analysis is a valuable tool for understanding the basic physicochemical properties of complex oxide materials and guiding their design to improve electrochemical performance and functionality in different energy storage applications.

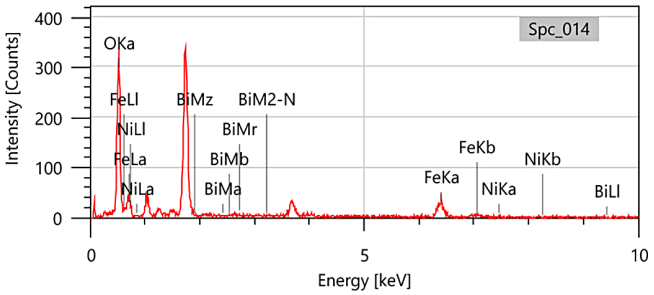

FIGURE 3 EDX spectra obtained during SEM scan. EDS, energy-dispersive X-ray spectroscopy; SEM, scanning electron microscopy

Using atomic force microscopy (AFM), we were able to gain a thorough understanding of the surface topography and morphology of the Ni-doped $BiFeO_3$ films that were deposited. This information is shown in Figure 5. Through the utilization of SEM and AFM imaging, the observed nanostructures were further confirmed via topographical view. It is interesting to observe the uniform

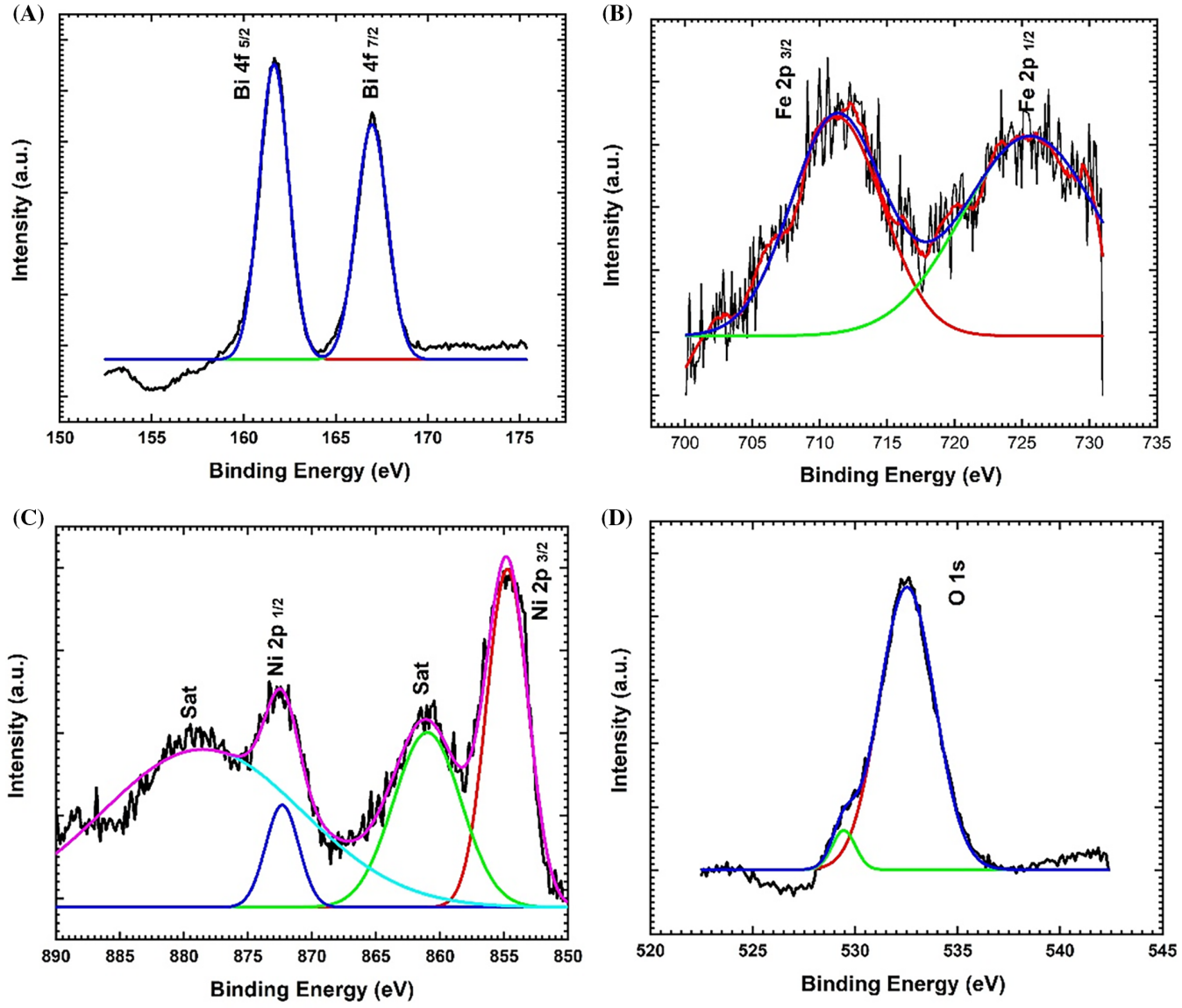

FIGURE 4 XPS spectra for the (A) Bi 4f, (B) Fe 2p, (C) Ni 2p, and (D) O 1s of the Ni doped $BiFeO_3$ thin film. XPS, X-ray photoelectron spectroscopy

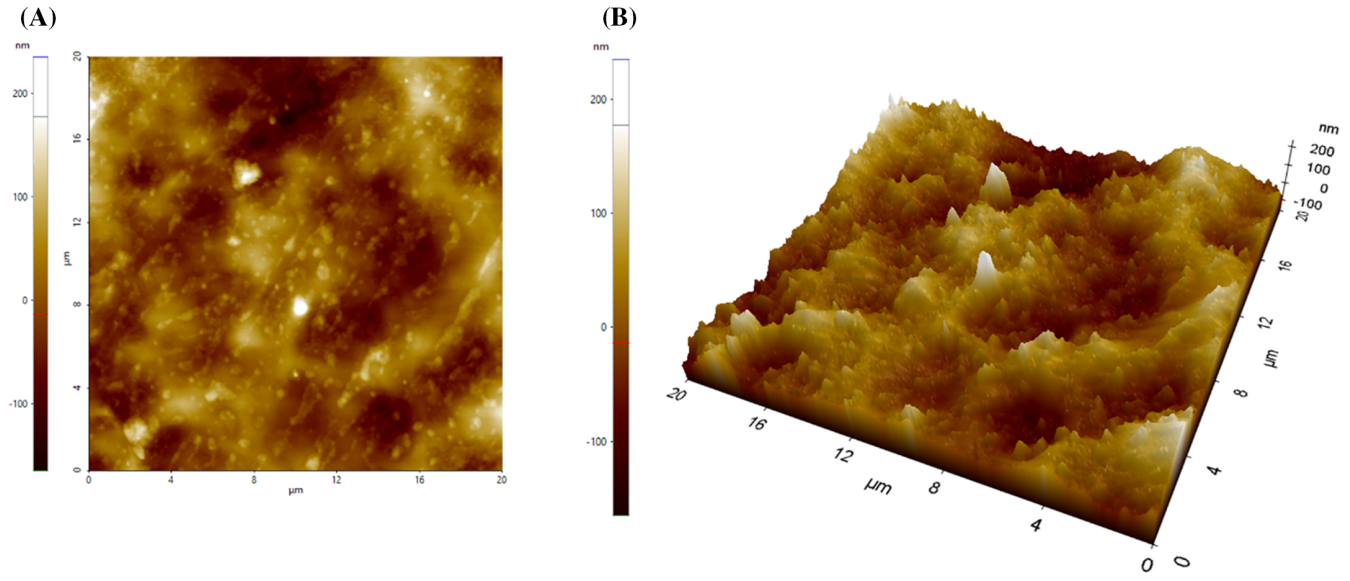

FIGURE 5 (A) 2D and (B) 3D AFM images of Ni doped $BiFeO_3$ thin films prepared by spray pyrolysis method. AFM, atomic force microscopy

structure of bismuth ferrite films, with an average height (Rz) ranging from 390.93 nm. In addition, the films' surface roughness was assessed using different parameters, including the root mean square value of roughness (Rq, 48.69 nm), root mean square of peak-valley depth (Rpv, 399.90 nm), and root mean square value of surface height deviation (Ra, 39.42 nm). This can be attributed to the enhanced surface diffusion of the grains. In addition, the Kurtosis value (Rku, 3.031) indicated a uniform formation of the structure, which aligns with previous findings from SEM imaging. This topographical information provides additional evidence that the annealing temperature used during film deposition was sufficient to induce the films to transition into a crystalline phase.[28] Additionally, the crystallization is highlighted, offering valuable insights for improving the fabrication process of Ni-doped $BiFeO_3$ films. These findings have important implications for a range of applications, such as electrochemical supercapacitors.

Through the analysis of the fingerprint region using Fourier-transform infrared spectroscopy (FTIR), significant information about the functional groups in nickel-doped bismuth ferrite ($BiFeO_3$) films was obtained, as shown in Figure 6. There were some significant transmittance peaks observed in the spectrum, particularly at 556 cm^{-1}. These peaks are believed to be caused by the bending and stretching vibrations of certain chemical bonds, specifically the O-Fe-O and Fe-O bonds.[29] These vibrations suggest the presence of the FeO6 octahedral structure. This observation highlights the existence of metal-oxygen bonds, which confirms the formation of the perovskite structure that is typical of $BiFeO_3$.[30] Furthermore, the peak observed at 674 cm^{-1} indicates the

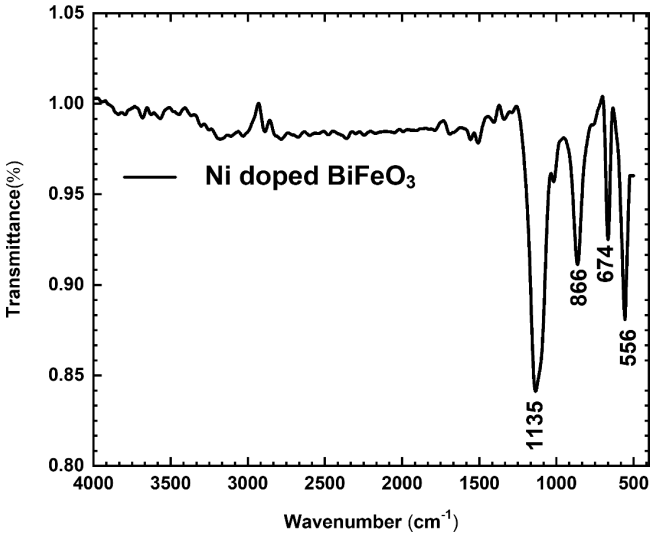

FIGURE 6 FTIR spectra of Ni-doped $BiFeO_3$ thin film in the wavenumber range of 500 to 4000 cm^{-1} at RT. FTIR, Fourier-transform infrared spectroscopy; RT, room temperature

vibration of oxygen atoms in a direction perpendicular to the (111) plane of the rhombohedral structure of BFO, providing additional evidence of the material's crystalline structure.[31] In addition, there are peaks observed at 866 cm^{-1} which indicate the bending vibrations of Bi_2O_3. This suggests that bismuth oxide has been incorporated into the octahedral structure of the material. These findings support the structural integrity of the synthesized films and emphasize the substitution of Ni^{2+} ions for Bi^{3+} ions, as indicated by the observed peaks that are characteristic of BFO with Ni doping.[32] In addition, the presence of a peak at 1135 cm^{-1} further confirms

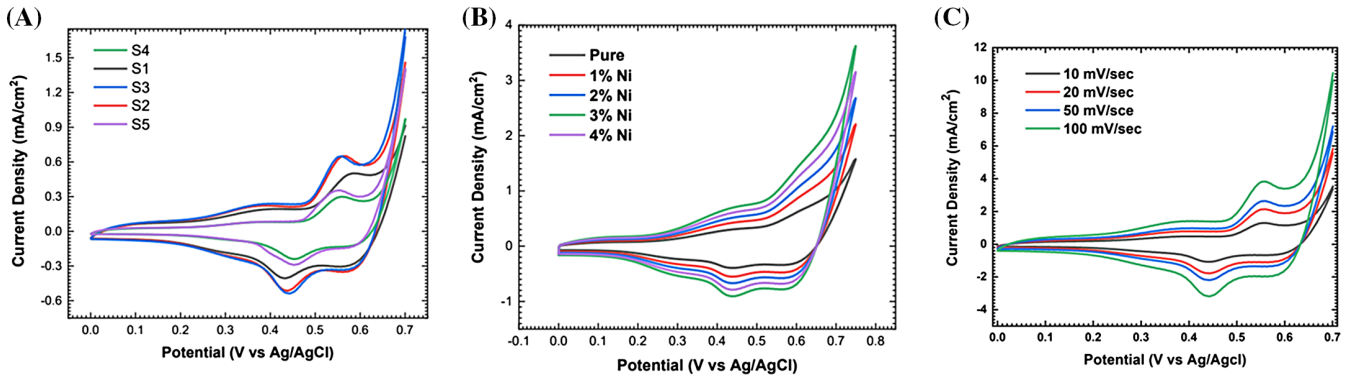

FIGURE 7 Cyclic voltammetry of (A) pure $BiFeO_3$, (B) Ni doped $BiFeO_3$, and (C) effect of scan rate on thin films deposited on FTO with variation of concentration

the crystalline nature of the films. This peak indicates the presence of well-organized atomic structures in the material, suggesting its crystalline nature. In analyzing the fingerprint region using FTIR, we gain valuable insights into the structure and composition of nickel-doped $BiFeO_3$ films. This information is crucial for understanding the properties and potential applications of these films in fields like electronics, catalysis, and energy storage.

2.1 | Cyclic voltammetry analysis

The electrochemical behavior of the $BiFeO_3$ electrode was examined using cyclic voltammetry (CV), the observation of its characteristics at various scan rates. The CV curve pure $BiFeO_3$ displayed in Figure 7A and Ni-doped $BiFeO_3$ in Figure 7B demonstrated remarkable capacitive behavior, characterized by rapid and reversible faradaic reactions. The observed redox peaks at specific potentials indicate the presence of effective surface charge storage mechanisms and pseudocapacitive characteristics.[33,34]

The analysis of CV performed on pristine $BiFeO_3$ using a three-electrode system at a potential window of 0 to 0.7 V revealed an intriguing trend in which the capacitance gradually increased as the synthesis concentrations increased. This rise started at 191.59 F/g and peaked at 0.03 M concentration. It continued to 253.31 F/g before declining further. This behavior indicates an ideal concentration (0.03 M) that promotes the highest charge storage capacity. Jadhav et al reported that the mixed phase BFO nanoflake for supercapacitor application with 72.2 F/g at current density of 1 A/g.[35] Some other comparative BFOs as supercapacitor applications are mentioned in Table 1.

In addition, the 0.03 M $BiFeO_3$ sample was doped with different percentages of Ni, resulting in a noticeable trend where capacitance increased in direct proportion to the doping percentage. It rises up to 312.12 F/g and after it decreases. The observed increase in capacitance upon Ni doping indicates an increase in conductivity, which in turn affects the material's charge storage capacity.[39,40] Afterward, an analysis using Electrochemical impedance spectroscopy (EIS) was performed to gain a deeper understanding of this phenomenon. The findings of the EIS study confirmed a clear link between higher doping levels of Ni and improved conductivity in the $BiFeO_3$ samples. The increase in conductivity was credited to the impact of Ni doping, which affected the transfer of charges and the movement of ions in the material, resulting in an improvement in its capacitance.[41,42] The relationship between the percentage of Ni doping, the improvement in conductivity, and the resulting effect on capacitance highlights the potential of Ni-doped $BiFeO_3$ as a promising option for high-performance energy storage applications.

Understanding the impact of scan rate on electrochemical supercapacitors is crucial as it influences various aspects of their performance, including ion diffusion, charge storage mechanisms, and electrode kinetics. With higher scan rates, the current densities tend to increase while the charge storage capacity decreases. This is because the ion diffusion becomes limited. In addition, higher scan rates can lead to increased charge transfer resistance and reduced capacitance retention over long cycles. Having a deep understanding of the scan rate is essential for improving the performance and lifespan of supercapacitors in a wide range of applications.

2.2 | Galvanostatic charge-discharge analysis

The galvanostatic charge-discharge (GCD) measurements for pure BFO, as shown in Figure 8A and Ni-doped BFO as shown in Figure 8B offer valuable insights into the charge storage capabilities of the $BiFeO_3$ electrode. The charge-discharge curves exhibited symmetrical and

Material	Capacitance	Capacitance retention	Ref.
BFO nanoflake	72.2 F/g @ 1 A/g	82% after 1500 GCD cycles	35
GCE/$BiFeO_3$	105 F/g @ 0.25 A/g	–	36
$Bi_{25}FeO_{40}$	351 F/g @ 4 A/g	–	37
BFO/graphene	9 mF/cm^2 @ 10 mV/s	95% after 5000 CV cycles	38
BFO ($BiFeO_3$)	312.12 F/g @ 10 mV/s	78% after 9000 GCD cycles	This work

Abbreviation: GCD, galvanostatic charge-discharge.

TABLE 1 A comparison of various BFO materials for supercapacitor application

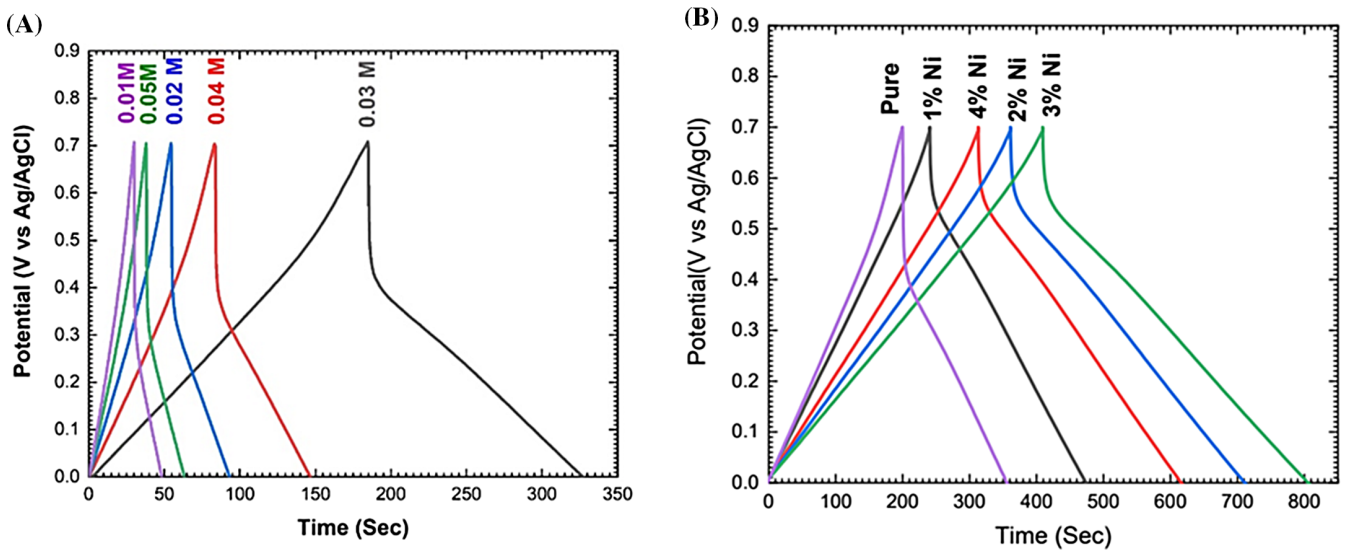

FIGURE 8 Galvanostatic charge-discharge of (A) pure $BiFeO_3$ and (B) Ni doped $BiFeO_3$ thin films deposited on FTO with variation of concentration

linear behavior, indicating a high specific capacitance and exceptional cycling stability. The specific capacitance values calculated at different current densities demonstrate the material's ability to maintain charge storage capacity under various operating conditions, highlighting its suitability for supercapacitor applications.

In the potential range of 0 to 0.7 V at 3 mA/cm^2 current density, the GCD test was conducted on pristine $BiFeO_3$. The charging time showed an upward trend with increasing concentrations from 49.8 to 329.27 s, peaking at 0.03 M concentration, and then declining up to 62.53 s. This trend is similar to the findings in CV studies. An increase in doping percentage was closely connected with a decrease in the abrupt potential drop after doping the 0.03 M $BiFeO_3$ sample with different percentages of Ni. This decrease in potential drop demonstrates enhanced charge-discharge properties due to improved conductivity resulting from the introduction of Ni.[43] The EIS analysis revealed valuable insights into the correlation between the levels of Ni doping and the conductivity of the material.[44] Through experimentation, it was discovered that increasing the Ni doping percentage has a positive effect on the conductivity of $BiFeO_3$. This, in turn, has an impact on the rate at which charge transfer occurs and the diffusion of ions within the material. The observed correlation between Ni doping levels, conductivity enhancement, and the resulting impact on the charge-discharge behavior demonstrates the potential of Ni-doped $BiFeO_3$ for optimized energy storage applications. This highlights the significance of fine-tuning the material's electrochemical properties to enhance its functionality in practical implementations. Also, cycle stability is an important feature of supercapacitors that can be used in real life,[45] so the cycling performance of the synthetic $BiFeO_3$ electrode was studied at a current density of 5 mA/cm^2. Based on 9000 cycles, the electrode exhibits 78% capacitance, indicating good capacitance retention, as shown in Figure 9B. This could also be credited to the exceptional structural and morphological design of the electrode material.

2.3 | EIS analysis

The analysis of the electrode's electrochemical behavior in the frequency domain is revealed through the EIS, as

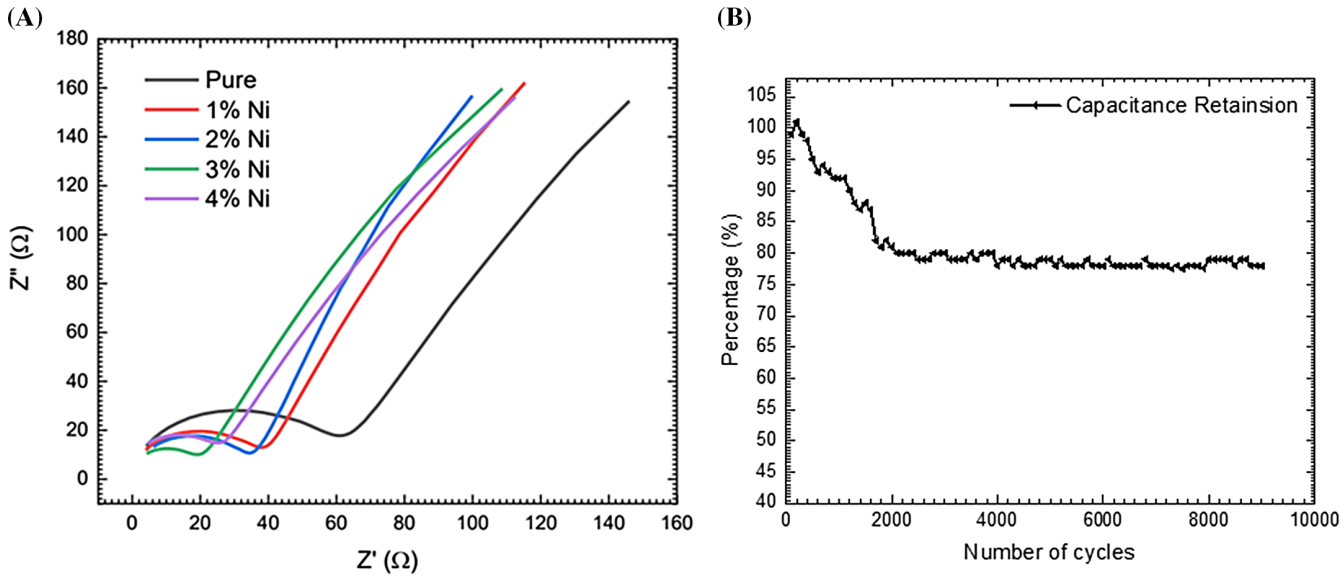

FIGURE 9 (A) Electrochemical impedance spectroscopy of pure and Ni doped $BiFeO_3$. (B) Capacitance retention studied by the GCD 9000 cycles. GCD, galvanostatic charge-discharge

TABLE 2 All synthesized samples are compared with mass loading, the resistance obtained from EIS analysis, and capacitance values

Sample code	Mass lading (mg)	R_{CT} (Ω)	R_B (Ω)	R_{Total} (Ω)	Capacitance (F/g)
S1	0.2	54.36	102.39	156.75	191.5989421
S2	0.3	48.20	98.11	146.31	242.4666088
S3	0.35	36.55	101.34	137.89	253.3189543
S4	0.4	47.12	96.20	143.32	214.5314225
S5	0.45	81.09	99.39	180.48	76.65267304
D1S3	0.30	42.8	91.79	134.59	221.6517216
D2S3	0.32	34.63	87.01	121.64	252.3267367
D3S3	**0.35**	**31.10**	**71.7**	**102.8**	**312.1218121**
D4S3	0.35	38.12	89.33	127.45	271.4102714

Note: The bold values represent the highest recorded capacitance values among the data presented.
Abbreviation: EIS, electrochemical impedance spectroscopy.

shown in Figure 9A. The Nyquist plots with small semicircles appearing at high frequencies and an inclined line at low frequencies. These patterns suggest that the charge transfer resistance is low and the ion diffusion kinetics within the $BiFeO_3$ electrode are excellent.[46] The observed impedance suggests that there are efficient ion diffusion processes at play, which contribute to improved charge storage performance.

The analysis performed on $BiFeO_3$ at 0.03 M concentration revealed specific conductivity characteristics. When adding different amounts of Ni to this 0.03 M $BiFeO_3$, we observed that the conductivity increased as the doping percentage increased. All the resistance, capacitance values are listed in Table 2. The increase in conductivity levels demonstrated the positive effect of introducing Ni into $BiFeO_3$, enhancing its electrical properties.[47] The increased conductivity resulting from higher Ni doping percentages significantly contributed to the enhancement of the material's overall performance. The increased conductivity allowed for more effective transfer of charges and faster diffusion of ions within the material.[48] The relationship between the rise in Ni doping percentages, the corresponding increase in conductivity, and the resulting improvement in electrochemical performance highlights the potential of Ni-doped $BiFeO_3$ as a highly promising material for advanced electrochemical applications. This realization emphasizes the significance of adjusting doping levels to enhance the electrical properties of $BiFeO_3$ for better performance in real-world electrochemical systems.

The improvement in overall performance seen with a 3% doping in the material can be credited to its capacity

to reduce charge transfer resistance in comparison to other doping percentages. With a deep understanding of materials, one can enhance electron transfer at the electrode-electrolyte interface, resulting in improved electrochemical performance. This includes higher specific capacitance and better rate capability. In addition, potential areas for future research could include analyzing the stability of materials over time and assessing their long-term performance and durability in different cyclic conditions. To enhance the electrochemical properties of the material, one could consider optimizing doping concentrations, exploring new electrode materials, and investigating advanced synthesis techniques. Furthermore, analyzing the stability of the material under various environmental conditions and cycling regimes can offer valuable insights into its durability and suitability for use in energy storage devices.

3 | CONCLUSION

The combined analysis integrating XRD, TEM, SEM, XPS, AFM, FTIR, and electrochemical studies provided comprehensive insights into $BiFeO_3$. XRD revealed a distorted rhombohedral structure conforming to the R3m (166) space group, complemented by TEM and SEM observations indicating a uniform thin-layer with additional confirmation by AFM topological analysis of morphology with beneficial void spaces, enhancing potential performance in energy storage. TEM and SEM further detailed $BiFeO_3$ NPs clustered within 50 to 70 nm, consistent with XRD data, while XPS confirmed acceptable Bi/Fe ratios comparable to prior studies. Electrochemical analyses unveiled intriguing concentration-dependent trends in capacitance and charging time, showing optimal behavior at 0.03 M concentration and suggesting Ni doping's impact on improving conductivity and charge-discharge characteristics. EIS elucidated the direct link between Ni doping levels and enhanced conductivity, emphasizing its role in facilitating improved charge transfer kinetics and ion diffusion. Together, these findings underline $BiFeO_3$'s promise for high-performance energy storage devices, emphasizing the need for controlled synthesis and doping strategies to maximize its electrochemical potential in practical applications.

CONFLICT OF INTEREST STATEMENT

The authors declare no conflicts of interest.

DATA AVAILABILITY STATEMENT

The data that support the findings of this study are available from the corresponding author- V. B. Ranmale, upon reasonable request.

ORCID

V. B. Ranmale https://orcid.org/0009-0002-9177-5719

REFERENCES

1. Dell RM, Rand DAJ. Energy storage—a key technology for global energy sustainability. *J Power Sources*. 2001;100(1):2-17. doi:10.1016/S0378-7753(01)00894-1
2. Gür TM. Review of electrical energy storage technologies, materials and systems: challenges and prospects for large-scale grid storage. *Energ Environ Sci*. 2018;11(10):2696-2767. doi:10.1039/C8EE01419A.10.1039/C8EE01419A
3. Afif A, Rahman SMH, Tasfiah Azad A, Zaini J, Islan MA, Azad AK. Advanced materials and technologies for hybrid supercapacitors for energy storage—a review. *J Energy Storage*. 2019;25:100852. doi:10.1016/j.est.2019.100852
4. Ramachandran T, Sana SS, Kumar KD, Kumar YA, Hegazy HH, Kim SC. Asymmetric supercapacitors: unlocking the energy storage revolution. *J Energy Storage*. 2023;73:109096. doi:10.1016/j.est.2023.109096
5. Mishra MK, Moharana S, Satpathy SK, et al. 12—Perovskite-type dielectric ceramic-based polymer composites for energy storage applications. *Perovskite Metal Oxides*. Elsevier; 2023:285-312. doi:10.1016/B978-0-323-99529-0.00014-X
6. Sun H, Wang X, Sun Q, et al. Large energy storage density in BiFeO3-BaTiO3-AgNbO3 lead-free relaxor ceramics. *J Eur Ceram Soc*. 2020;40(8):2929-2935. doi:10.1016/j.jeurceramsoc.2020.03.012
7. Selvaraj Y, Kuzhandaivel H, Nallathambi KS, Elayappan V. Enhanced cyclic stability of cobalt doped Bi25FeO40/BiFeO3 as an electrode material for a super long life symmetric supercapacitor device. *Energy Fuel*. 2023;37(12):8624-8636. doi:10.1021/acs.energyfuels.3c00135
8. Yin L, Mi W. Progress in BiFeO3-based heterostructures: materials, properties and applications. *Nanoscale*. 2020;12(2):477-523. doi:10.1039/C9NR08800H
9. Charishma VD, Shastrimath V, Bairy R, et al. Materials today. *Proceedings*. 2021;35:440-444. doi:10.1016/j.matpr.2020.02.950
10. Nagashree MC, Kulkarni SD, Rajendra BV, Seidel J, Murari MS, Sharma P. Spray pyrolysis-derived robust ferroelectric BiFeO3thin films. *Phys Chem Chem Phys*. 2023;25(33):22286-22293. doi:10.1039/D3CP02877A
11. Rana G, Dhiman P, Kumar A, et al. Recent advances on nickel nano-ferrite: a review on processing techniques, properties and diverse applications. *Chem Eng Res Des*. 2021;175:182-208. doi:10.1016/j.cherd.2021.08.040
12. Adhikari S, Mandal S, Kim D-H. Recent development strategies for bismuth-driven materials in sustainable energy systems and environmental restoration. *Small*. 2023;19(10):2206003. doi:10.1002/smll.202206003
13. Belousov AS, Suleimanov EV. Application of metal–organic frameworks as an alternative to metal oxide-based photocatalysts for the production of industrially important organic chemicals. *Green Chem*. 2021;23(17):6172-6204.
14. Fawzi AS, Sheikh AD, Mathe VL. Structural, dielectric properties and AC conductivity of Ni(1−x)ZnxFe2O4 spinel ferrites. *J Alloys Compd*. 2010;502(1):231-237.
15. Ferri EAV, Santos IA, Radovanovic E, Bonzanini R, Girotto EM. Chemical characterization of BiFeO3 obtained by Pechini method. *J Braz Chem Soc*. 2008;19:1153-1157.

16. Zhu C, Chen Z, Zhong C, et al. Facile synthesis of BiFeO3 nanosheets with enhanced visible-light photocatalytic activity. *J Mater Sci Mater Electron*. 2018;29(6):4817-4829. doi:10.1007/s10854-017-8437-6
17. Rani S, Shekhar M, Kumar P, Prasad S. Study on quantitative Rietveld analysis of XRD patterns of different sizes of bismuth ferrite. *Appl Phys A*. 2022;128(12):1046. doi:10.1007/s00339-022-06171-y
18. Wani WA, Kundu S, Ramaswamy K, Venkataraman H. Structural, morphological, optical and dielectric investigations in cobalt doped bismuth ferrite nanoceramics prepared using the sol-gel citrate precursor method. *J Alloys Compd*. 2020;846:156334. doi:10.1016/j.jallcom.2020.156334
19. Betancourt-Cantera LG, Bolarín-Miró AM, Cortés-Escobedo CA, Hernández-Cruz LE, Sánchez-de Jesús F. Structural transitions and multiferroic properties of high Ni-doped BiFeO3. *J Magn Magn Mater*. 2018;456:381-389.
20. Nakano K, Oka K, Watanuki T, et al. Glassy distribution of Bi3+/Bi5+in Bi1−xPbxNiO3 and negative thermal expansion induced by intermetallic charge transfer. *Chem Mater*. 2016;28(17):6062-6067.
21. Alshaaer M, Issa K, Afify AS, et al. The Impact of Full-Scale Substitution of Ca2+ with Ni2+ Ions on Brushite's Crystal Structure and Phase Composition. *Crystals*. 2022;12(7):940.
22. Wei Q, Xiong F, Tan S, et al. Porous one-dimensional nanomaterials: design, fabrication and applications in electrochemical energy storage. *Adv Mater*. 2017;29(20):1602300. doi:10.1002/adma.201602300
23. Nadeem M, Khan W, Khan S, et al. Significant enhancement in photocatalytic performance of Ni doped BiFeO3 nanoparticles. *Mater Res Express*. 2018;5(6):065506.
24. Fominykh K, Chernev P, Zaharieva I, et al. Iron-doped nickel oxide nanocrystals as highly efficient electrocatalysts for alkaline water splitting. *ACS Nano*. 2015;9(5):5180-5188.
25. Basith NM, Vijaya JJ, Kennedy LJ, Bououdina M. Structural, morphological, optical, and magnetic properties of Ni-doped CuO nanostructures prepared by a rapid microwave combustion method. *Mater Sci Semicond Process*. 2014;17:110-118.
26. Chen L, Li C, Zhao Y, et al. Constructing 3D Bi/Bi4O5I2 microspheres with rich oxygen vacancies by one-pot solvothermal method for enhancing photocatalytic activity on mercury removal. *Chem Eng J*. 2021;425:131599.
27. Liu R, Shi Y, Lin L, et al. Surface Lewis acid sites and oxygen vacancies of Bi2WO6 synergistically promoted photocatalytic degradation of levofloxacin. *Appl Surf Sci*. 2022;605:154822.
28. Zhao Z, Li H. Effects of deposition potential and anneal temperature on the hexagonal nanoporous nickel hydroxide films. *Chem Mater*. 2007;19(16):3882-3891.
29. Lehnert N, Ho RYN, Que L, et al. Spectroscopic properties and electronic structure of low-spin Fe(III)−Alkylperoxo complexes: homolytic cleavage of the O−O bond. *J Am Chem Soc*. 2001;123(34):8271-8290.
30. Chchiyai Z, El Bachraoui F, Tamraoui Y, et al. Design, structural evolution, optical, electrical and dielectric properties of perovskite ceramics Ba1-xBixTi1-xFexO3 ($0 \leq x \leq 0.8$). *Mater Chem Phys*. 2021;273:125096.
31. Rao TD, Asthana S, Niranjan MK. Observation of coexistence of ferroelectric and antiferroelectric phases in Sc substituted BiFeO3. *J Alloys Compd*. 2015;642:192-199.
32. Crumpton TE, Mosselmans JFW, Greaves C. Structure and oxide ion conductivity in Bi28Re2O49, a new bismuth rhenium oxide containing tetrahedral and octahedral Re(vii). *J Mater Chem*. 2005;15(1):164-167.
33. Costentin C, Porter TR, Savéant J-M. How do pseudocapacitors store energy? Theoretical analysis and experimental illustration. *ACS Appl Mater Interfaces*. 2017;9(10):8649-8658. doi:10.1021/acsami.6b14100
34. Wu D, Kang Y, Wang F, et al. Surface-redox pseudocapacitance-dominated charge storage mechanism enabled by the reconstructed cathode/electrolyte interface for high-rate magnesium batteries. *Adv Energy Mater*. 2023;13(40):2301145. doi:10.1002/aenm.202301145
35. Jadhav VV, Zate MK, Liu S, et al. Mixed-phase bismuth ferrite nanoflake electrodes for supercapacitor application. *Appl Nanosci*. 2016;6(4):511-519. doi:10.1007/s13204-015-0469-8
36. Matinise N, Botha N, Madiba IG, et al. Mixed-phase bismuth ferrite oxide (BiFeO3) nanocomposites by green approach as an efficient electrode material for supercapacitor application. *MRS Adv*. 2023;8(12):703-707. doi:10.1557/s43580-023-00603-4
37. Kumar AM, Ragavendran V, Mayandi J, Ramachandran K, Jayakumar K. Phase dependent electrochemical characteristics of bismuth ferrite: a bifunctional electrocatalyst for supercapacitors and dye-sensitized solar cells. *Colloids Surf A Physicochem Eng Asp*. 2023;656:130529. doi:10.1016/j.colsurfa.2022.130529
38. Soam A, Kumar R, Mahender C, et al. Development of paper-based flexible supercapacitor: bismuth ferrite/graphene nanocomposite as an active electrode material. *J Alloys Compd*. 2020;813:152145. doi:10.1016/j.jallcom.2019.152145
39. Krishnan SG, Archana PS, Vidyadharan B, et al. Modification of capacitive charge storage of TiO2 with nickel doping. *J Alloys Compd*. 2016;684:328-334. doi:10.1016/j.jallcom.2016.05.183
40. Ramesh S, Karuppasamy K, Yadav HM, et al. Ni(OH)2-decorated nitrogen doped MWCNT nanosheets as an efficient electrode for high performance supercapacitors. *Sci Rep*. 2019;9(1):6034. doi:10.1038/s41598-019-42281-z
41. Li W, Liu J, Zhao D. Mesoporous materials for energy conversion and storage devices. *Nat Rev Mater*. 2016;1(6):16023. doi:10.1038/natrevmats.2016.23
42. Raccichini R, Varzi A, Passerini S, Scrosati B. The role of graphene for electrochemical energy storage. *Nat Mater*. 2015;14(3):271-279. doi:10.1038/nmat4170.10.1038/nmat4170
43. Das HT, Mahendraprabhu K, Maiyalagan T, et al. Performance of solid-state hybrid energy-storage device using reduced graphene-oxide anchored sol-gel derived Ni/NiO nanocomposite. *Sci Rep*. 2017;7(1):15342. doi:10.1038/s41598-017-15444-z
44. Laschuk NO, Easton EB, Zenkina OV. Reducing the resistance for the use of electrochemical impedance spectroscopy analysis in materials chemistry. *RSC Adv*. 2021;11(45):27925-27936. doi:10.1039/d1ra03785d
45. Salanne M, Rotenberg B, Naoi K, et al. Efficient storage mechanisms for building better supercapacitors. *Nat Energy*. 2016;1(6):16070. doi:10.1038/nenergy.2016.70
46. Tripathi HS, Dutta A, Sinha TP. Tailoring structural and electrochemical properties in Sr2+ incorporated nanostructured BiFeO3 for enhanced asymmetric solidstate supercapacitor. *Electrochim Acta*. 2022;421:140505. doi:10.1016/j.electacta.2022.140505

47. Nadeem M, Khan W, Khan S, Husain S, Ansari A. Tailoring dielectric properties and multiferroic behavior of nanocrystalline BiFeO3 via Ni doping. *J Appl Phys*. 2018;124(16):164105. doi:10.1063/1.5050946
48. Maier J. Nanoionics: ion transport and electrochemical storage in confined systems. *Nat Mater*. 2005;4(11):805-815. doi:10.1038/nmat1513

How to cite this article: Ranmale VB, Kadam LD, Shinde TJ. Exploring the influence of Ni doping thin films for supercapacitor application. *Energy Storage*. 2024;6(4):e637. doi:10.1002/est2.637